

RESEARCH ARTICLE

10.1002/2017JA024615

Solar Illumination Control of the Polar Wind

L. Maes^{1,2}, R. Maggiolo¹, J. De Keyser^{1,3}, M. André⁴, A. I. Eriksson⁴, S. Haaland^{2,5}, K. Li^{6,7}, and S. Poedts³

Key Points:

- Polar wind flux density exhibits a dependence on the solar zenith angle
- Both density and velocity in the polar wind show similar but weaker solar zenith angle dependence
- Seasonal variations are observed in the polar wind flux density

Supporting Information:

- Supporting Information S1
- Figure S1

Correspondence to:

L. Maes,
maes@mps.mpg.de

Citation:

Maes, L., Maggiolo, R., DeKeyser, J., André, M., Eriksson, A. I., Haaland, S., ... Poedts, S. (2017). Solar illumination control of the polar wind. *Journal of Geophysical Research: Space Physics*, 122, 11,468–11,480. <https://doi.org/10.1002/2017JA024615>

Received 21 JUL 2017

Accepted 4 NOV 2017

Accepted article online 9 NOV 2017

Published online 26 NOV 2017

¹Royal Belgian Institute for Space Aeronomy, Brussels, Belgium, ²Max Planck Institute for Solar System Research, Göttingen, Germany, ³Center for Mathematical Astrophysics, KU Leuven, Leuven, Belgium, ⁴Swedish Institute for Space Physics, Uppsala, Sweden, ⁵Department of Physics and Technology, University of Bergen, Bergen, Norway, ⁶Key Laboratory of Earth and Planetary Physics, Institute of Geology and Geophysics, Chinese Academy of Sciences, Beijing, China, ⁷State Key Laboratory of Space Weather, Chinese Academy of Sciences, Beijing, China

Abstract Polar wind outflow is an important process through which the ionosphere supplies plasma to the magnetosphere. The main source of energy driving the polar wind is solar illumination of the ionosphere. As a result, many studies have found a relation between polar wind flux densities and solar EUV intensity, but less is known about their relation to the solar zenith angle at the ionospheric origin, certainly at higher altitudes. The low energy of the outflowing particles and spacecraft charging means it is very difficult to measure the polar wind at high altitudes. We take advantage of an alternative method that allows estimations of the polar wind flux densities far in the lobes. We analyze measurements made by the Cluster spacecraft at altitudes from 4 up to 20 R_E . We observe a strong dependence on the solar zenith angle in the ion flux density and see that both the ion velocity and density exhibit a solar zenith angle dependence as well. We also find a seasonal variation of the flux density.

1. Introduction

The polar ionosphere is a special region because it is connected magnetically to the magnetic field in the solar wind. On the closed magnetic field lines that thread the lower latitude ionosphere a near-hydrostatic equilibrium is established in the trapped plasma of the plasmasphere, but on the open magnetic field lines of the polar ionosphere this is not possible, and ions keep flowing out (Dessler & Michel, 1966; Nishida, 1966). The term *polar wind* was coined by Axford (1968), in analogy to the solar wind. Being less heavy, the ionospheric electrons can escape more easily than the ions so that an ambipolar electric field parallel to the magnetic field lines is set up to maintain quasi-neutrality, accelerating the ions upward (Dessler & Cloutier, 1969; Lemaire & Scherer, 1969, 1970).

This ambipolar electric field is weak but nonetheless manages to cause a significant amount of ions to escape. Its flux (please see the note on our use of the terms “flux” and “flux density” in the beginning of section 2) is estimated at 10^{25} to 10^{26} s^{-1} (André et al., 2015; Cully et al., 2003; Engwall, Eriksson, Cully, André, Puhl-Quinn, et al., 2009; Engwall, Eriksson, Cully, André, Torbert, et al., 2009; Huddlestone et al., 2005; Nagai et al., 1984). As a consequence, the magnetospheric lobes are filled by this steady flow of low-energy ions (André & Cully, 2012; Engwall, Eriksson, Cully, André, Puhl-Quinn, et al., 2009). Ions flowing on these open magnetic field lines can escape into interplanetary space, and thus, the polar wind acts as a sink for ionospheric and magnetospheric plasma. Not all ions flowing out through the lobes manage to escape the magnetosphere, however, since convection transports them perpendicularly to the magnetic field lines so that ions with too low parallel velocities compared to the convection velocity will end up in the plasma sheet (e.g., Ebihara et al., 2006). Haaland et al. (2012) estimated that on average only 10% of the ions flowing through the lobes manage to escape into the solar wind directly.

Not only polar wind ions flow in the lobes but also ions energized in the cusp pass through the lobes. Compared to the rest of the magnetic polar cap, there is a large energy input into the cusp in the form of Poynting flux and particle precipitation (Moore & Khazanov, 2010; Nilsson et al., 2012; Strangeway et al., 2005). Therefore, despite its small spatial extent, the cusp is a significant source of ion outflows, which have been estimated to be of the order of 10^{25} s^{-1} (Nilsson et al., 2012; Pollock et al., 1990; Yau & André, 1997). Ions flowing out from the cusp can be convected over the polar cap into the lobes and mix with the polar wind, so that it can be difficult to differentiate between “classical” polar wind ions and cusp ions.

Solar illumination is the main source of energy driving the polar wind. Consequently, several studies have found that the flux density in the lobes increases when the solar extreme ultraviolet (EUV) radiation (parametrized by $F_{10.7}$) intensifies (André et al., 2015; Cully et al., 2003; Engwall, Eriksson, Cully, André, Puhl-Quinn, et al., 2009). The solar illumination received by the ionosphere does not only vary with the intensity of the solar EUV radiation but also with the elevation of the Sun, which can be parametrized by the solar zenith angle (SZA). This has received less attention in observational polar wind studies, however. Su, Horwitz, Moore, et al. (1998) observed a sharp drop of the densities from SZA of 90° to 105° . Abe et al. (1993, 2004) also found the polar wind velocity to go down as the SZA goes up. Models of the polar wind that include hot photoelectrons predict similar behavior (e.g., Glocer et al., 2012; Su, Horwitz, Wilson, et al., 1998). In a study of outflowing ions above small-scale polar cap arcs, Maes et al. (2015) reported a strong drop of flux densities around SZA of $\sim 100^\circ$ and argued that these flux densities should be similar to polar wind flux densities. Note that the flux densities in the lobes have also been found to be affected by geomagnetic activity (see, e.g., André et al., 2015; Cully et al., 2003; Engwall, Eriksson, Cully, André, Puhl-Quinn, et al., 2009; Haaland et al., 2015; Yau et al., 1988).

The solar zenith angle dependence of the electron density above the polar cap has also been studied. Johnson and Wygant (2003), Nsume et al. (2008), and Kitamura et al. (2011) all found that at lower altitudes (roughly below $2 R_E$ altitude) the electron density strongly depends on the SZA. The former two, however, found that at altitudes above $4 R_E$ there was no discernible SZA effect, and geomagnetic activity (parametrized by the Kp index) was the determining factor.

Most measurements of the polar wind have been done at altitudes not much higher than $\sim 10,000$ km, because at higher altitudes the low-energy ions of the polar wind become increasingly difficult to measure. A spacecraft traveling through space is exposed to EUV radiation that knocks electrons away from its surface. If the density of the ambient plasma is not high enough to compensate for this flux of electrons away from the spacecraft, like at high altitudes in the lobes, the spacecraft will acquire a positive charge. In the lobes this spacecraft potential can go up to several tens of volts. Since polar wind ions typically have energies only of the order of a few eV, they cannot overcome the spacecraft potential and do not reach the detectors. For this reason they are often referred to in literature as “cold ions.” The instruments on the Polar spacecraft managed to make measurements of the polar wind at altitudes of $8 R_E$ using a system actively reducing the spacecraft potential down to 1 or 2 V (Moore et al., 1997; Su, Horwitz, Moore, et al., 1998). This type of potential control, however, can only be used for a limited amount of time, and the ions with energy below the reduced spacecraft potential are still missed.

An alternative approach was used by Engwall et al. (2006). By exploiting the spacecraft potential to find the plasma density (Pedersen et al., 2001) and the charged wake created behind the spacecraft (Eriksson et al., 2006) to estimate the ion bulk velocity, they managed to measure the polar wind flux densities. This method requires a specific set of electric field experiments, as is present on the Cluster spacecraft (Escoubet et al., 1997), and has resulted in several investigations of the polar wind in the magnetospheric lobes and polar cap region (see Haaland et al., 2016, for an overview). This is also the method used by André et al. (2015) to compile the data set used in this study. It will be explained in some detail in the next section. It has the advantage that it can measure polar wind fluxes with low energies at high altitudes, theoretically without a lower limit on the energy. It can also be used over extended periods of time and is thus suitable for statistical studies. A downside of the method is that it requires the presence of a wake behind the spacecraft caused by the supersonic flow of cold ions, which is not always the case.

The goal of this paper is to assess the effect of the solar zenith angle of the ionospheric origin on the polar wind flux density at high altitudes. In what follows we will first introduce the experimental methods and discuss the data characteristics in section 2. In section 3 we report the results, and we will discuss them and their implications in section 4.

2. Data and Method

The main quantity we want to study is the flux density. This is the product of the ion density and the ion bulk velocity, which can be found for cold ions with the two alternative methods explained in sections 2.1 and 2.2, respectively. Please note that the terms “flux” and “flux density” may be used with a different meaning in other texts. We use the term flux for a quantity integrated over an area and flux density for the differential quantity.

Then the dimensions of a particle flux become $[T]^{-1}$ and of flux density $[L]^{-2}[T]^{-1}$. This has the advantage of being consistent with the terminology of electromagnetism as well as with current and current density.

In order to be able to compare flux densities from different altitudes, we normalize them to a reference altitude of 200 km, by dividing them by the ratio of the magnetic field strength measured by the spacecraft over magnetic field strength at 200 km altitude. Note that this choice of reference altitude is arbitrary and different from many other studies which may normalize to different altitudes (often higher), and this should be taken into account when comparing the flux densities with those from other studies.

The Cluster mission consists of four spacecraft launched into a $4 \times 19 R_E$ polar orbit in July and August 2000 (Escoubet et al., 1997). Among the set of instruments on board of each spacecraft are two electric field experiments that use different principles, and it is this specific combination that allows this method to find the ion bulk velocity. The Electric Field and Wave (EFW) instrument utilizes two probes mounted on long wire booms (Gustafsson et al., 1997) with a probe-to-probe distance of 88 m. This instrument therefore measures the electric field on a scale of the order of the length of the booms. The Electron Drift Instrument (EDI) emits and recaptures a beam of electrons and acquires the electric field from the drift of the gyration center of the electrons in the beam (Paschmann et al., 1997). Since the energy of the emitted electrons is 0.5 or 1 keV, their gyroradius in the lobes is of the order of a few kilometers, and thus, this method will not be affected by electric field variations at smaller scales.

2.1. Plasma density: Spacecraft Potential

If the density of the plasma surrounding a spacecraft is not high enough to compensate the current to the spacecraft carried by the photoelectrons emitted from its surface, the spacecraft will acquire a positive charge. This prevents ions with too low energy to overcome the resulting spacecraft potential to reach the onboard instruments. The magnitude of the spacecraft potential depends on the solar irradiance, spacecraft properties (like shape, surface material, and area), and the plasma density. With due calibration, the spacecraft potential can therefore be used to determine the plasma density (Lybekk et al., 2012; Pedersen et al., 2001, 2008). Typically, the density n can be written as an exponential function (or superposition thereof) of the spacecraft potential V_{sc} . For this data set the relation

$$n(t, V_{sc}) = \phi(t) A e^{\frac{-V_{sc}}{B}} \quad (1)$$

is used. This is the relation given by Lybekk et al. (2012) but additionally multiplied with a normalization function $\phi(t)$ to account for daily variations in the irradiance. $\phi(t)$ is given by the value of $F_{10.7}$ at time t divided by the average $F_{10.7}$ of the year of t , that is, $\phi(t) = \frac{F_{10.7}(t)}{\langle F_{10.7} \rangle_{\text{year}}}$. The parameters A and B are given for specific ranges of V_{sc} and years. They can be found in Lybekk et al. (2012).

This method determines the electron density, which, by assumption of quasi-neutrality and singly charged ions (which holds for ions of ionospheric origin), is equal to the total ion density. This method cannot distinguish between different ion species.

2.2. Ion Bulk Velocity: Wake Electric Field

The polar wind, at a certain altitude, reaches supersonic speeds (Nagai et al., 1984), and an object moving through a medium at supersonic speeds creates a wake behind it. In a plasma, electrons can more easily enter this wake than ions because of the electrons' typically higher thermal speed. This charge separation sets up an electric field. When a spacecraft is charged, the wake forms behind the electrostatic structure surrounding the spacecraft and is typically much larger than the spacecraft dimension (Eriksson et al., 2006). This enhanced wake occurs when the kinetic energy associated with bulk flow of the ions is smaller than the energy needed to overcome the spacecraft potential, but larger than the ions' thermal energy, that is, when

$$kT_i < \frac{m_i v_i^2}{2} < eV_{sc}, \quad (2)$$

where T_i , m_i , and v_i are the ion temperature, mass, and bulk flow, respectively, and V_{sc} is the spacecraft potential, and k is the Boltzmann constant.

EDI is unaffected by the small-scale electric field due to the wake behind the spacecraft, and thus, the electric field measured by it is the ambient convection electric field. The electric field measured by the EFW experiment, on the other hand, is a superposition of the large-scale convection electric field and the wake electric field. Therefore, the wake electric field can be found from their difference: $\mathbf{E}^w = \mathbf{E}^{EFW} - \mathbf{E}^{EDI}$. Assuming the

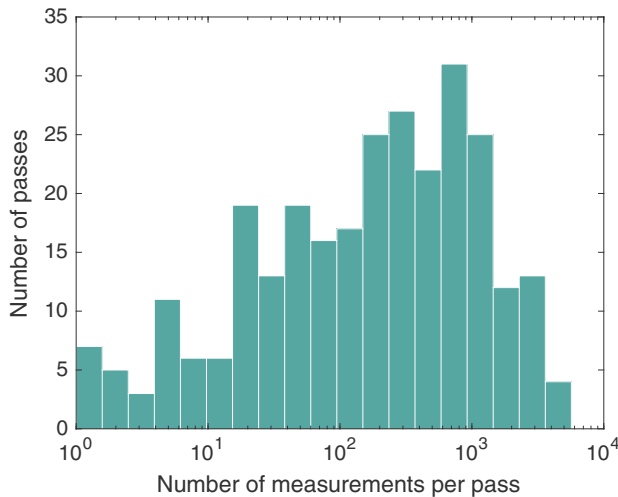


Figure 1. Distribution of number of measurements per pass.

ions are unmagnetized on the scale of the wake, the electric field \mathbf{E}^w is in the direction of the plasma flow \mathbf{v} and may be written as

$$\mathbf{E}^w = g\mathbf{v} = g\mathbf{v}_\perp + gv_\parallel \frac{\mathbf{B}}{B}, \quad (3)$$

where g is some scalar function which may depend on the plasma properties or the plasma flow speed v but is independent of the flow direction (Engwall et al., 2006; Engwall, Eriksson, Cully, André, Puhl-Quinn, et al., 2009). If the frozen-in condition applies, the perpendicular component of the flow velocity should be the convection velocity and can thus be found from the electric field measured by EDI: $\mathbf{v}_\perp = \mathbf{E}^{EDI} \times \mathbf{B}/B^2$.

EFW can only measure the electric field in the spin plane of the spacecraft; however, this is no problem as long as the projection of \mathbf{E}^w onto the spin plane is not too small. Decomposing \mathbf{E}^w into components E_x^w and E_y^w in the spin plane, an expression for v_\parallel is found by dividing equation (3) for one component by that for the other and rearranging:

$$v_\parallel = \frac{E_x^w v_{\perp,y} - E_y^w v_{\perp,x}}{E_y^w B_x - E_x^w B_y} B. \quad (4)$$

Note that it is unnecessary to know the scalar function g . If there is a significant population of hot ions coexisting with the cold ions, this method does not work since the hot ions can enter the wake and thus cancel it out.

Note also that other studies using the same method multiply the density with a factor of 0.8 (assuming a fixed composition of 80% H^+ ions), and then only discuss H^+ ions, to compensate for the fact that heavier ions at the same velocity will have a higher energy and thus more likely violate the requirements of equation (2) (see Engwall, Eriksson, Cully, André, Puhl-Quinn, et al., 2009). However, as long as the ions' energy satisfies equation (2), the method should work regardless of the composition. For this reason, as well as because in this study we are not interested in the absolute outflow but in its variation with SZA (and thus a constant factor for all densities is irrelevant and has no impact on our results or conclusions), we choose not to assume a particular composition and do not multiply the densities with 0.8.

2.3. Data

The data set used in this study is a subset of the one compiled by André et al. (2015). The original data set contains data from both Cluster 1 and Cluster 3. To select the data, several constraints were introduced to guarantee the quality of the data, which can be found in the appendix of André et al. (2015).

In the present study, however, we will only use data from Cluster 1, for reasons mentioned in Appendix A. This subset consists of more than 160,000 individual measurements in the magnetospheric lobes at altitudes between 4 and 20 R_E over a period spanning from July 2001 until July 2009. Due to the orbit of Cluster measurements in the lobes could only be made during the months July to November. These measurements come from 282 passes, of which 142 in the northern lobe and 140 in the southern lobe. Within these passes, the majority of the measurements are 4 s apart, which is the spacecraft spin period, but there are also larger gaps up to several hours. Most of the passes have less than 1,000 measurements, but some have more, up to 5,680. The distribution of the number of measurements per pass is shown in Figure 1. There are no measurements in 2008 and only two passes (in the southern lobe) in 2009 (in July). The data set covers a large part of the solar cycle. As a result, there is a large range of EUV intensity, and the $F_{10.7}$ index ranges from 71.2 solar flux units (sfu) up to 285.5 sfu, with a median of 134.4 sfu.

2.4. Solar Zenith Angle

To find the solar zenith angle of the ionospheric origin of the ions, we use the Tsyganenko 89 model (Tsyganenko, 1989) to trace the magnetic field line from the spacecraft's position down to the ionosphere, at an altitude of 200 km. It is important to note that this is no particle tracing; that is, all movement perpendicular to the magnetic field lines is neglected. Therefore, convection may be a cause of error on the determined solar zenith angle. We will discuss its possible effect on our results in section 4.2.

For ions flowing at the velocities as found in the data, the transport time from ionosphere to the position of the spacecraft may be on the order of an hour. We chose not to introduce any correction for this, since the correct

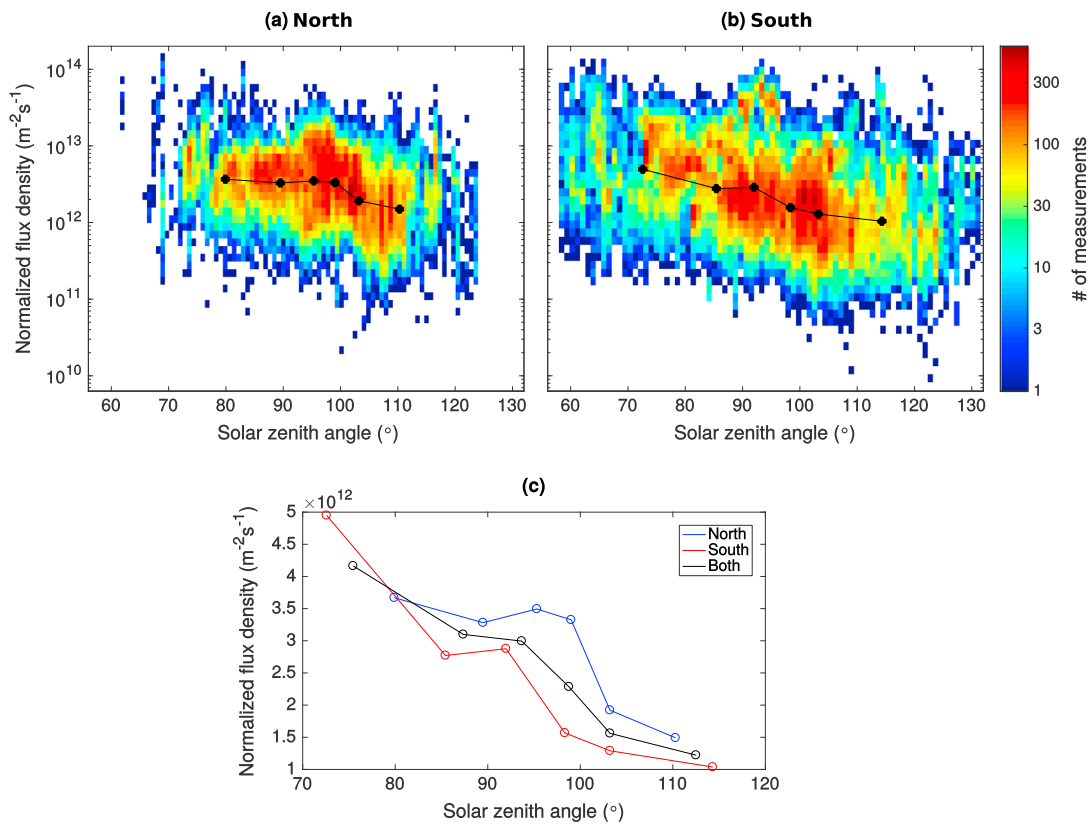


Figure 2. Flux density versus SZA. The bivariate distributions of the (normalized) flux density (on the y axis) and the SZA (on the x axis), for the (a) northern and (b) southern hemispheres. The black dotted line shows the average per equal amount of sorted data. (c) The averages on a linear scale.

determination of the transport time would require knowledge of the exact path, the altitude of acceleration, etc. These are all unknown or very difficult to establish, and thus, trying to correct for the transport time would significantly increase the complexity of the data and its assumptions for little to no increase in precision.

We checked the results using several methods for estimating the transport time (including using velocity and distance and constant transport time), and the overall conclusions do not change. Moreover, the error due to the neglect of the perpendicular motion is most likely much larger.

We also divide the data according to hemisphere. Because of the constant motion of the magnetotail, the northern and southern hemispheric lobes cannot be found by simply looking at the z_{GSM} coordinate. Therefore, the hemisphere to which the measurements belong is determined by the projection of the magnetic field onto the spacecraft position vector: north if this is negative, south if it is positive.

3. Results

Figures 2a and 2b show the bivariate distributions of the normalized flux densities (on the y axis) and solar zenith angle (on the x axis), for the northern and southern hemispheres, respectively. The color scale shows the number of measurements in each bin. The black line is the average of groups of equal number of data points sorted according to SZA. In Figure 2c these averages are shown again, but on a linear scale, in blue and red for the northern and southern hemispheres, respectively, and black for both hemispheres combined. A downgoing trend, from low to high SZA, can clearly be seen. The average flux density in both hemispheres in Figure 2c decreases by a factor of more than 3 from small to large SZA, going from $4.2 \times 10^{12} \text{ s}^{-1} \text{ m}^{-2}$ to $1.2 \times 10^{12} \text{ s}^{-1} \text{ m}^{-2}$.

In order to check the statistical significance of the variation of the flux density over the SZA, we divide the data into two groups according to their SZA, more specifically, a group with SZA smaller than 100° and a group with SZA larger than 100° . We choose this value, because, due to the transparency of the atmosphere, the terminator at ionospheric altitude will be at SZA larger than 90° , and 100° falls in the ranges found for the

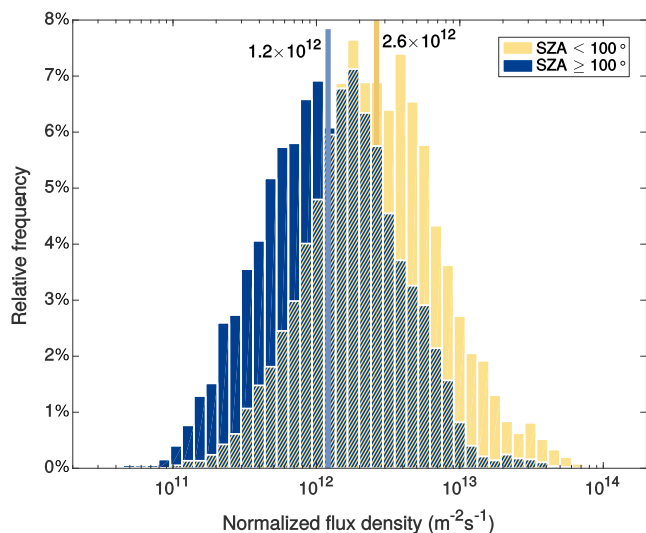


Figure 3. Distribution of the (normalized) flux densities, split up according to SZA. The thinner blue and yellow lines give the logarithmic average of both distributions.

transition region in several studies (Glocer et al., 2012; Maes et al., 2015; Su, Horwitz, Wilson, et al., 1998; Su, Horwitz, Moore, et al., 1998). In order to have independent values, we use the averages per 160 s, as explained in Appendix A. The distributions of the flux densities of both groups can be seen in Figure 3. They are close to a lognormal distribution. The statistical significance of the difference between the averages of both distributions is high. When performing a Mann-Whitney-Wilcoxon test (Cooper, 1969), even with the reduced data set, the probability that both sets come from the same distribution is smaller than 10^{-15} .

Since the flux density is the product of the density and the velocity, it is interesting to see whether it is the density or the velocity that causes the dependency of the flux on the solar zenith angle. Therefore, the same type of bivariate histograms as for the flux are shown for the density (normalized to 200 km altitude using the magnetic field in the same way as done for the flux density) in Figure 4, and for the velocity in Figure 5. From this we see that both the density and the velocity depend on the solar zenith angle. Together they combine to the flux density, which has an even clearer dependency on the SZA.

The average normalized density for both hemispheres at the smallest SZA, $1.4 \times 10^8 \text{ m}^{-3}$, is more than double that at the largest SZA, $7.0 \times 10^7 \text{ m}^{-3}$. The velocity goes from 29 km s^{-1} at small SZA down 17 km s^{-1} at large SZA. This is a decrease with a factor of 1.7 (or a decrease with a factor of 2.9 in terms of the corresponding kinetic energy).

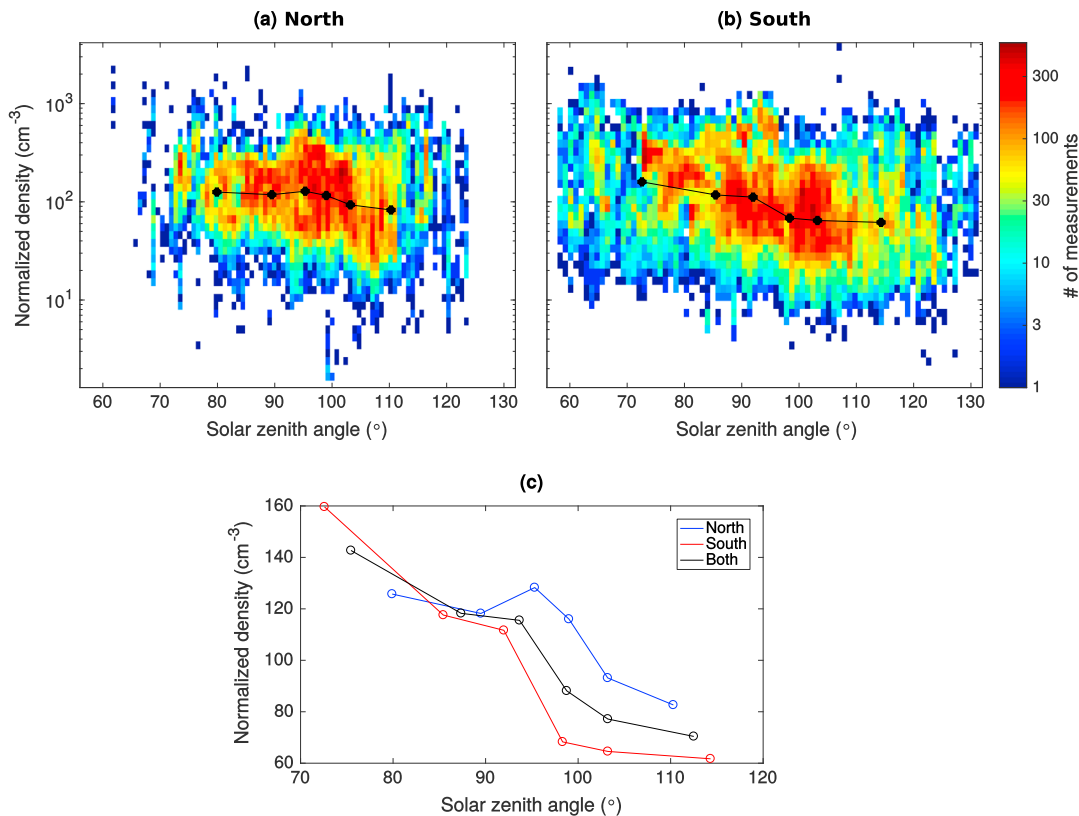


Figure 4. Density versus SZA. The bivariate distributions of the (normalized) density (on the y axis) and the SZA (on the x axis), for the (a) northern and (b) southern hemispheres. The black dotted line shows the average per equal amount of sorted data. (c) The averages on a linear scale.

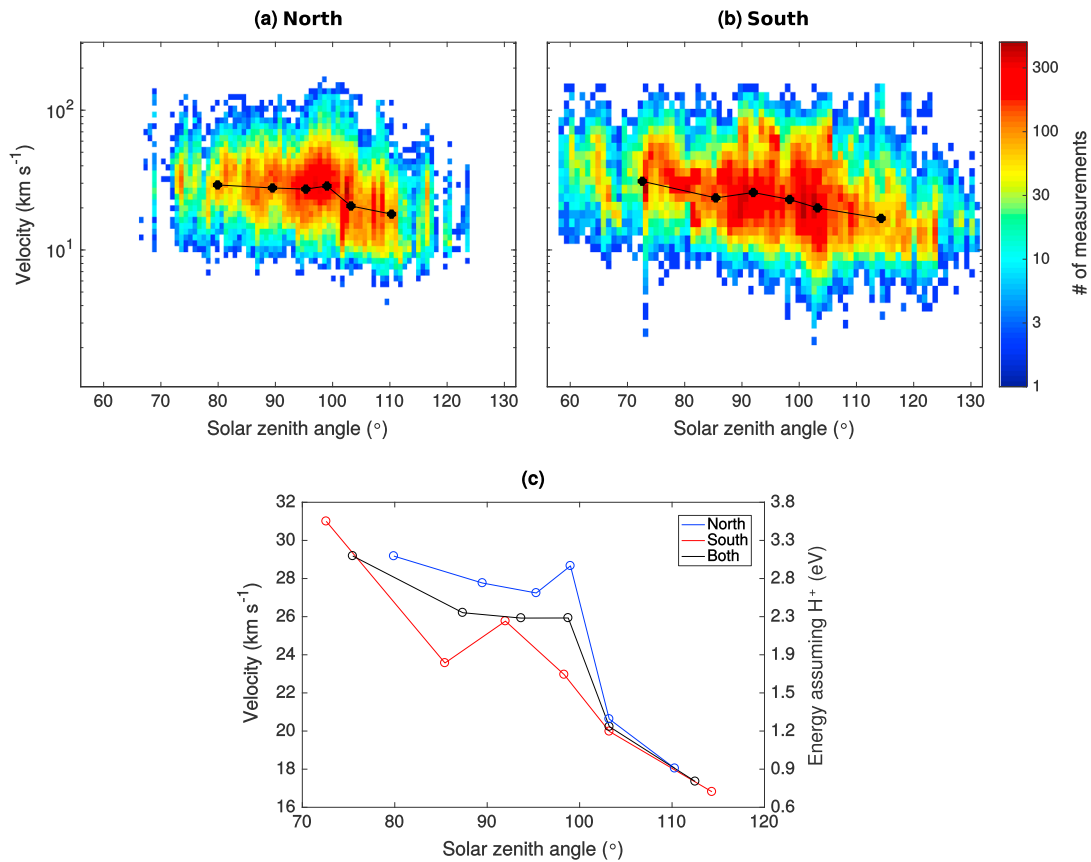


Figure 5. Velocity versus SZA. The bivariate distributions of the velocity (on the y axis) and the SZA (on the x axis), for the (a) northern and (b) southern hemispheres. The black dotted line shows the average per equal amount of sorted data. (c) The averages on a linear scale.

The magnetospheric lobes are magnetically connected to the magnetic polar caps. And since the magnetic polar cap rotates on a seasonal (and diurnal) basis, the SZA of the mapped spacecraft positions has a time dependency. Therefore, one might also expect a similar time dependency of the flux densities. Figure 6 shows the bivariate histograms of the flux densities and the time of year. This figure collects data covering more than 8 years. As mentioned in section 2, all the data come from the months July till November.

An overall trend going from low to high flux densities can be seen for the southern hemisphere in Figures 6b and 6c. This is as one would expect for a hemisphere going from its summer solstice to its winter solstice. For the northern hemisphere a downward trend can be seen to some extent, as expected for a hemisphere going from its summer solstice to its winter solstice, although there is a large peak in September.

For both hemispheres the seasonal trend is much less clear than for the SZA. This is to be expected, since the SZA does not depend solely on the day of year but also on the position in the polar cap and on the time of the day.

4. Discussion

Before we draw conclusions from these results, it is important to understand how biases or sampling issues in the data can affect the results shown in section 3. We discuss this in section 4.1 and continue with the interpretation of the results in section 4.2.

4.1. Effect of Statistical Issues

The unevenly distributed number of measurements per pass, as evidenced in Figure 1, causes some statistical difficulties. The plasma conditions during passes with much more measurements may be overrepresented if all single measurements are given equal weight. The effect one pass with many measurements can have on the statistics should not be underestimated. For example, in Figure 2b, the red or orange patch around 95° and $4 \times 10^{13} \text{ m}^{-2} \text{ s}^{-1}$ is completely caused by one pass at 21 October 2001 with 1744 measurements.

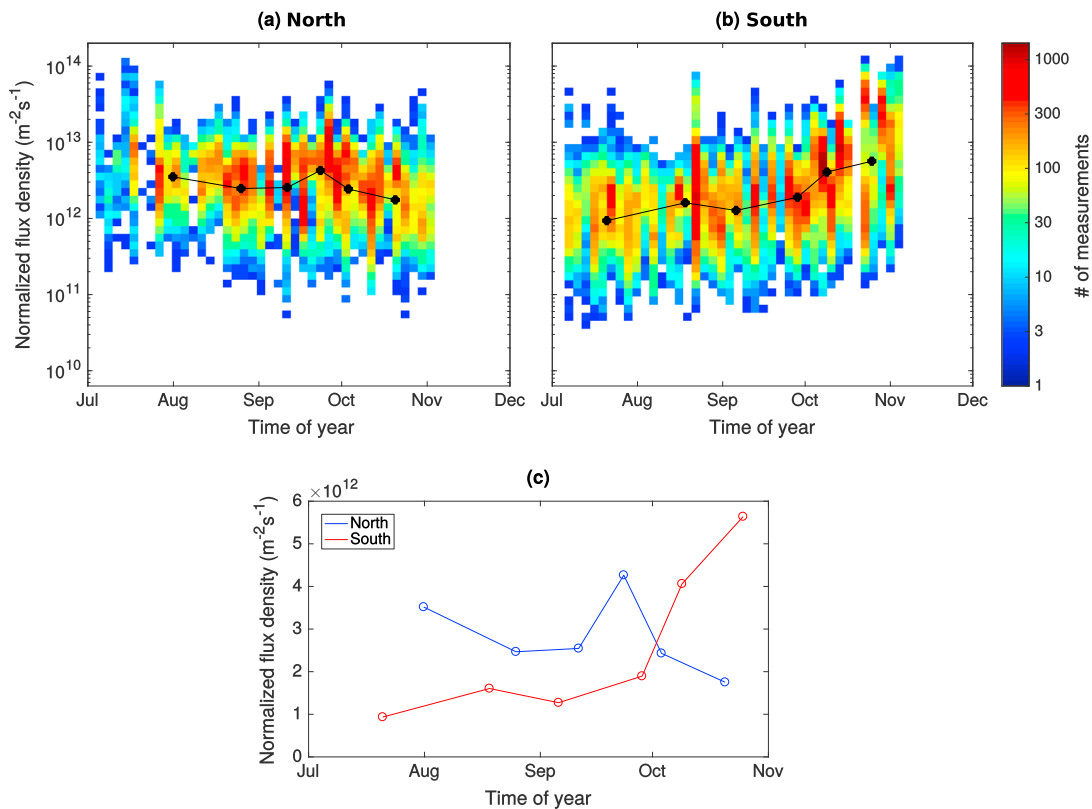


Figure 6. Flux density versus time. The bivariate distributions of the (normalized) flux density (on the y axis) and the time of year (on the x axis), for the (a) northern and (b) southern hemispheres. The black dotted line shows the average per equal amount of sorted data. (c) The averages on a linear scale.

Similarly, in Figure 2a, the red bump between 94° and 99° is almost completely caused by one pass at 23 September 2001 with 3815 measurements (of which ~2900 within the bump). To illustrate the effect passes like this can have on the averages, we show in Figure 7 the same averages as in Figure 2c, but without these two passes. Considering their relatively high velocity, it is not unlikely that the ions in these events are cusp outflow convected across the polar cap, rather than polar wind outflow.

This issue is even worse for the time variation, since a single pass may be spread over several SZA, but it will always be concentrated in a period of several hours. The large peak at September for the northern hemisphere is to a large extent (but not completely) caused by that same pass at 23 September 2001.

There is also an orbital bias such that there are more measurements in the later months (September–November) from the earlier years (2001–2003) and more measurements in the earlier months (July–August) from the later years (2005–2007). Since the solar cycle was around its maximum in 2001–2003, and close to its minimum during the years 2005–2007, there is also some bias in $F_{10.7}$. The data in the first half of the time range (in day of year), that is, before approximately 3 September, has an average $F_{10.7}$ that is 54 sfu lower than that in the second half in the northern hemisphere, and 42 sfu in the southern. Since $F_{10.7}$ has also been shown to affect the ion outflow, this may weaken the seasonal variation in the north and strengthen it in the south.

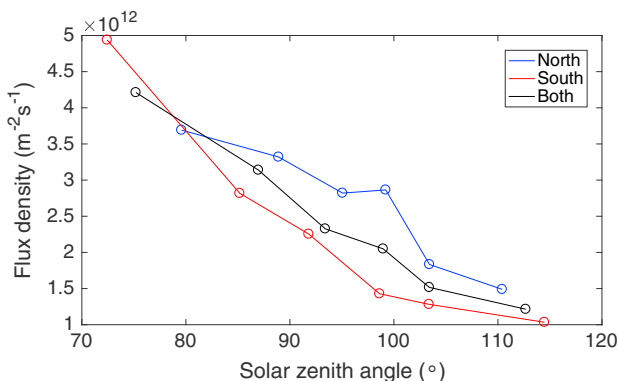


Figure 7. The average fluxes as in Figure 2c, but with the passes of 23 September 2001 and 21 October 2001 eliminated.

Since there is a correlation between the season and the solar zenith angle (although, oppositely for north and south), one might expect this bias in $F_{10.7}$ to propagate into the SZA. For the northern hemisphere, the average $F_{10.7}$ for the data with a SZA smaller than ~94°, that is, the middle of the SZA range, is 19 sfu lower than the data with a larger SZA. For the southern hemisphere, the average $F_{10.7}$ for the smaller SZA group is 11 sfu higher. The bias is thus smaller for the SZA but may again weaken

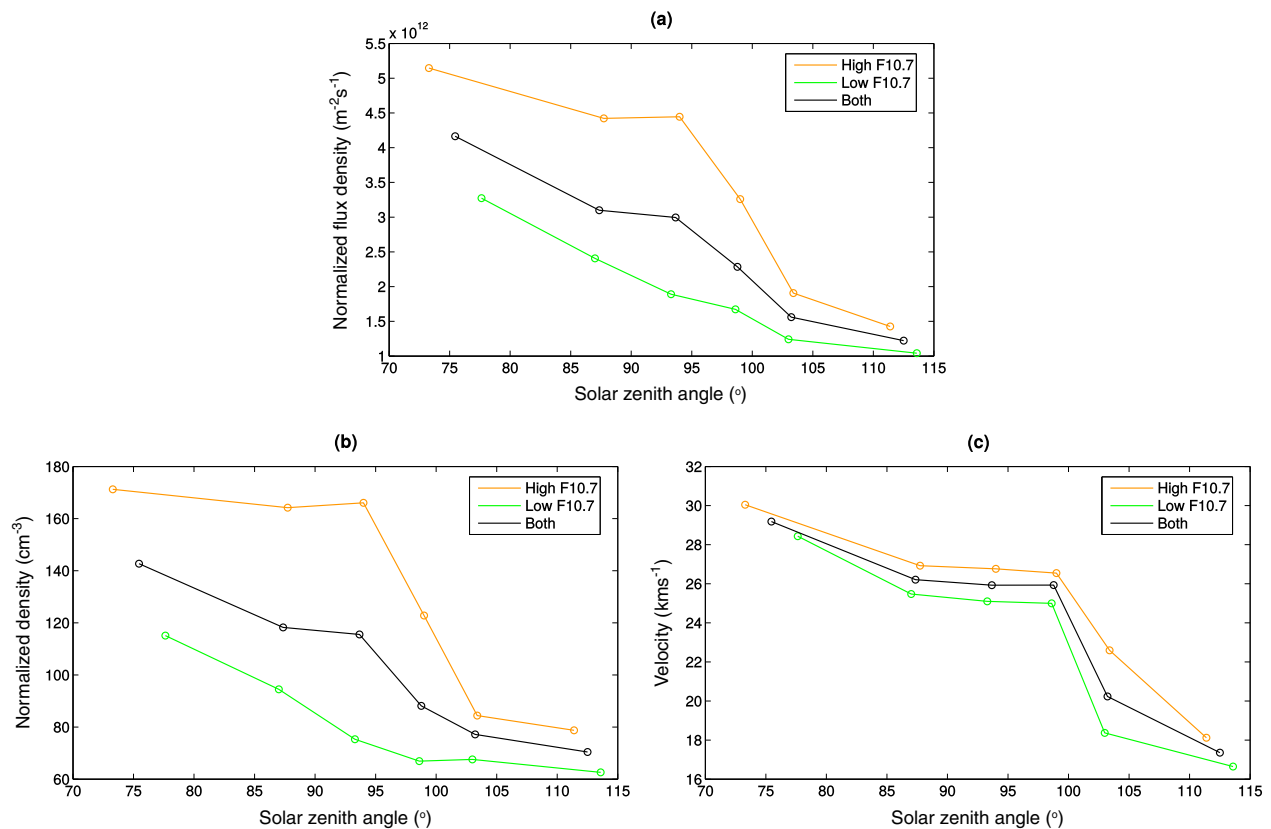


Figure 8. High and low $F_{10.7}$. The average per equal amount of sorted data, split up according to $F_{10.7}$, are shown in (a) the flux density, (b) the density, and (c) the velocity. The green line is the average for $F_{10.7}$ lower than or equal to 134.4 sfu, the orange line for $F_{10.7}$ higher than 134.4 sfu, and the black line for all data.

the effect in the north and strengthen it in the south. For all data combined, the average $F_{10.7}$ for the smaller SZA group is 4 sfu lower.

To further separate the SZA effect from the $F_{10.7}$ effect, we split up the data in two groups and plot the flux density, density, and velocity against the SZA in Figure 8. The averages are shown in green for the data with $F_{10.7}$ lower than the median (134.4 sfu), in orange for the data with $F_{10.7}$ higher than the median, and in black for all data. It is clear that the SZA effect is still present for both groups.

4.2. Interpretation

Figure 2 shows clear evidence of the importance of the solar zenith angle of the ionospheric origin for the ion flux densities in the magnetospheric lobes. This is similar to what Maes et al. (2015) find for the ion outflow above small-scale polar cap arcs, both in flux density and in its response to solar illumination. This finding thus seems to agree with the suggestion of Maes et al. (2015) that the flux densities of the polar wind and of ion outflows above small-scale polar cap arcs are comparable. No dependence of the flux densities on the x_{SM} coordinate of the ionospheric origin was found (a figure evidencing this can be found in the supporting information), suggesting that the distance to the cusp is not an important factor and that the data set is thus not overly contaminated by cusp outflow. The typically higher energy of cusp outflow makes it less likely for a detectable wake behind the spacecraft to be created, which is how many cusp outflow events may be filtered out of our “cold ion” data set (note that a wake is detected in the lobes approximately 65–70% of the time (André et al., 2015; Engwall et al., 2009)).

The velocity modulation by the SZA witnessed in Figure 5 agrees with the observations by Akebono reported by Abe et al. (1993, 2004). The change of the density over the SZA evidenced in Figure 4 is in concordance with the findings of Su, Horwitz, Moore, et al. (1998) with Polar data for H^+ . It is also in agreement with the fact that ionospheric electron densities at low altitudes above the polar caps are very strongly affected by the SZA (Johnson & Wygant, 2003; Kitamura et al., 2011; Nsumei et al., 2008). At altitudes above $4 R_E$, on the other hand,

Johnson and Wygant (2003) and Nsume et al. (2008) did not find an effect of SZA but found geomagnetic activity to be more important. There is a plausible explanation for this discrepancy. As also suggested by these authors, at higher altitudes the influence of convected cusp outflow (i.e., the so-called cusp or cleft ion fountain) becomes more important. Therefore intense cusp outflow events, which will correlate well with geomagnetic activity, may drown out the SZA effect of the low-energy polar wind. As mentioned before, many of these cusp outflow events are likely not in our data set, so that we are able to observe the SZA effect of the polar wind.

The large uncertainty on the SZA due to convection may be a cause of error, but we can make a rough estimate of its impact on our results. Convection can be antisunward, stagnant, or even sunward, but typical convection velocities at ionospheric altitudes have an antisunward component of 250 m s^{-1} (Förster et al., 2007). The median altitude of all measurements is roughly $10 R_E$ and the median outflow velocity 24 km s^{-1} . This gives a travel time of 44 min, which will change the SZA by 5.6° . So we find that convection causes a smoothing of the SZA on the order of 5° , although individual errors may be larger. This will blur the relation between the flux density and the SZA. The fact that we still see a relation, despite the error due to convection, is all the more evidence that there really is one.

A difference between our study and the Maes et al. (2015) and Su, Horwitz, Moore, et al. (1998) studies is that the latter both find two regimes, that is, outflow above a sunlit and a dark ionosphere, with a relatively small transition between both (at least for O^+). Figure 2c suggests more a gradual change over the SZA. However, as explained above, the large uncertainty on the SZA due to convection would most likely blur any sharp transition that may be present. This is much less the case for the outflows above the small polar cap arcs, since they have been accelerated strongly by the associated electric field (Maggiolo et al., 2011, 2012), which largely decreases the possible impact of convection. Similarly, the results from Su, Horwitz, Moore, et al. (1998) come from measurements at $\sim 5,000 \text{ km}$ altitude, where convection will have had less time to play a role. Since the polar wind is dominated by H^+ ions, one may find Figure 3 to be comparable to Figure 2b in Maes et al. (2015), which also shows the distributions split up according to SZA smaller or larger than 100° . However, considering this uncertainty on the SZA, it is most likely not possible to conclude much about the nature of the transition, that is, gradual or sharp.

Solar illumination has an important impact on the ionosphere. It heats the ionosphere, increases the ionospheric density, and may create hot photoelectrons. The variation of the outflowing flux density with the solar zenith angle is a sign that the state of the local ionosphere determines (at least in part) the outflowing flux densities. This corroborates the conclusion by André et al. (2015) that the cold ion fluxes in the magnetospheric lobes are mostly limited by the ion supply from the ionosphere. In Figure 8b, we see also that $F_{10.7}$ has a large effect on the density in the outflow at small SZA, but only a small or no effect at large SZA. This makes sense since a variation in solar illumination intensity can only have an effect on a position in the ionosphere if that position indeed also receives solar illumination.

Interestingly, though, while André et al. (2015) did find a variation of both the density and the flux density with $F_{10.7}$, they reported no significant change of the velocity over different values of $F_{10.7}$. We do find a variation of the velocity with the SZA. Figure 8c also confirms that there is an effect of SZA, but no (significant) effect of $F_{10.7}$. This may be of interest as to how solar illumination affects the ion outflow.

A density increase in the ion outflow may be attributed to an increase in the ionospheric density or an increased ambipolar electric field (since it reaches down into the ionosphere). An increase of the velocity may be due to an increased ambipolar electric field or due to acceleration by additional mechanisms like centrifugal acceleration or wave activity (which typically only occur higher up in the magnetosphere). The solar zenith angle of the ionospheric origin is unlikely to affect energization mechanisms like centrifugal acceleration or wave activity, though, so that the former cause seems the only likely explanation. Solar illumination may alter the ambipolar electric field by increasing the ionospheric temperature and by producing hot photoelectrons. The latter is suggested by some studies to have an important effect on the ambipolar electric field (e.g., Gloer et al., 2012; Khazanov et al., 1997; Su, Horwitz, Wilson, et al., 1998). At lower solar zenith angles the ionospheric density will be higher (Friedrich et al., 2006; Kitamura et al., 2011), which leads to a higher density of the ionospheric outflow. At lower solar zenith angles the ionospheric temperature (and especially that of the electrons) will be higher as well (Kitamura et al., 2011), so that the ambipolar electric field will be stronger, and thus also the outflowing velocity will be higher.

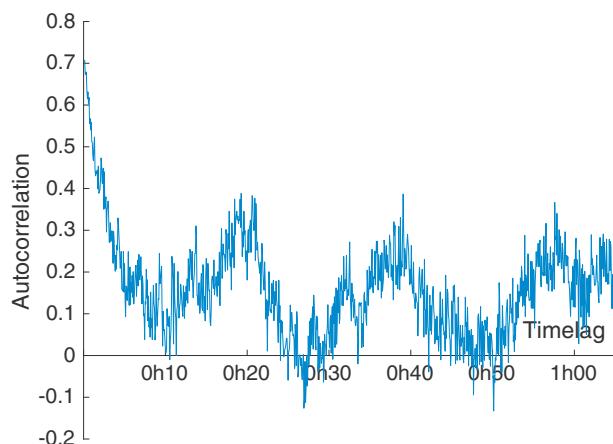


Figure A1. Autocorrelation function of the flux density during an example pass through the northern lobe on 24 August 2003.

Despite all the statistical issues with uneven sampling and the bias in $F_{10.7}$, we do also find a seasonal trend in the southern hemisphere, and a less convincing trend in the northern hemisphere, as was predicted by, for example, Maes et al. (2016). This is further evidence for the impact of solar illumination on the ion outflow via modulation of the ionosphere.

5. Conclusions

We have analyzed a large data set with cold ion flux densities measured at altitudes of 4 to 20 R_E in the magnetospheric lobes. We can make several conclusions:

1. The flux density exhibits a dependence on the solar zenith angle.
2. The density and velocity show a similar but less strong dependence and together combine to the stronger dependence of the flux density.
3. Due to the correlation between solar zenith angle and the season, we also observe a seasonal variation in the flux density.

These findings corroborate the idea that the state of the local ionosphere is the main factor determining the polar wind number flux density and that solar illumination has an important role in this. The density of the ionosphere may be altered as well as the ambipolar electric field of the polar wind.

Appendix A: Independent Measurements

Due to the nature of the method, working with this data requires that one keeps certain issues in mind. Apart from the measurement error, which was already discussed in André et al. (2015), and the effect of the large variety of number of measurements per pass, which was discussed in section 4.1, there is also the issue of independence of measurements. Since most of the individual measurements are only 4 s apart, they have also been made close to each other in space and thus cannot be considered independent measurements. Therefore, we should not overestimate the statistical significance this large number of measurements suggests. Many statistical constructs and tests, like the standard error (or the interpretation thereof), hypothesis tests, or correlation coefficients, assume independent measurements. The autocorrelation of the flux density for a particular pass shown in Figure A1 demonstrates this problem. The autocorrelation does not behave the same for all passes, but what almost all of them have in common is this initial sharp drop of the autocorrelation. For many of them this sharp drop is at some point intercepted by a slower decreasing curve or often even going upward again toward a peak, suggesting some sort of quasiperiodicity in the data. The example shown in Figure A1 even has multiple peaks at more or less equidistant time lags, which would suggest some periodicity with multiple harmonics.

We interpret the initial drop as the drop in autocorrelation due to measurements being taken progressively farther apart and thus becoming more and more independent. It is unlikely that the other behavior can be explained this way and thus most likely this has some other cause. There may be a physical explanation, like variation of the density due to compression of the lobes or movement of the magnetotail caused by variations in solar wind pressure or Kelvin-Helmholtz waves. We did not investigate this, however. It may be an interesting subject for a further study.

In order to acquire independent measurements, we define a time t_c as the time for which the autocorrelation first drops below 0.5, so that the coefficient of autodetermination becomes lower than 0.25. The average $\langle t_c \rangle$ for all orbits is 160 s, and this is larger than the t_c of 90% of the passes. Therefore, when performing statistical tests, we will average the measurements per 160 s intervals and treat these as individual independent measurements.

This issue with independent measurements is also why we chose to work with data from one spacecraft only. Using data from a second spacecraft in the same region in space at the same time would introduce again similar problems with independence of the measurements.

Acknowledgments

This work was supported by the Interuniversity Attraction Pole Planet TOPERS initiated by the Belgian Science Policy Office. J. D. K. and R. M. acknowledge the support of the Solar-Terrestrial Centre of Excellence and the Belgian Science Policy Office and ESA through PRODEX PEA C4000109739 and PEAC4000119635. S. H. acknowledges the support by the Research Council of Norway/CoE under contracts 223252/F50 and Deutsches Zentrum für Luft-und Raumfahrt, grant 50OC1401. M. A. and A. E. acknowledge the support by SNSB (Swedish National Space Board) contracts 72/12 and 170/12. All data from the EDI and FGM instruments are available at the Cluster Science archive (CSA), and EFW data are available at CSA and via M. André (mats.andre@irfu.se).

References

- Abe, T., Whalen, B. A., Yau, A. W., Horita, R. E., Watanabe, S., & Sagawa, E. (1993). EXOS D (Akebono) suprathermal mass spectrometer observations of the polar wind. *Journal of Geophysical Research*, *98*(11), 11,191–11,203. <https://doi.org/10.1029/92JA01971>
- Abe, T., Yau, A. W., Watanabe, S., Yamada, M., & Sagawa, E. (2004). Long-term variation of the polar wind velocity and its implication for the ion acceleration process: Akebono/suprathermal ion mass spectrometer observations. *Journal of Geophysical Research*, *109*, A09305. <https://doi.org/10.1029/2003JA010223>
- André, M., & Cully, C. M. (2012). Low-energy ions: A previously hidden solar system particle population. *Geophysical Research Letters*, *39*, L03101. <https://doi.org/10.1029/2011GL050242>
- André, M., Li, K., & Eriksson, A. I. (2015). Outflow of low-energy ions and the solar cycle. *Journal of Geophysical Research: Space Physics*, *120*, 1072–1085. <https://doi.org/10.1002/2014JA020714>
- Axford, W. I. (1968). The polar wind and the terrestrial helium budget. *Journal of Geophysical Research*, *73*, 6855–6859. <https://doi.org/10.1029/JA073i021p06855>
- Cooper, B. E. (1969). *Statistics for experimentalists* (pp. 273–276). Oxford, UK: Pergamon. <https://doi.org/10.1016/B978-0-08-012600-5.50017-9>
- Cully, C. M., Donovan, E. F., Yau, A. W., & Arkos, G. G. (2003). Akebono/Suprathermal Mass Spectrometer observations of low-energy ion outflow: Dependence on magnetic activity and solar wind conditions. *Journal of Geophysical Research*, *108*, 1093. <https://doi.org/10.1029/2001JA009200>
- Dessler, A. J., & Cloutier, P. A. (1969). Discussion of letter by Peter M. Banks and Thomas E. Holzer, "The polar wind". *Journal of Geophysical Research*, *74*, 3730–3733. <https://doi.org/10.1029/JA074i014p03730>
- Dessler, A. J., & Michel, F. C. (1966). Plasma in the geomagnetic tail. *Journal of Geophysical Research*, *71*, 1421–1426. <https://doi.org/10.1029/JZ071i005p01421>
- Ebihara, Y., Yamada, M., Watanabe, S., & Ejiri, M. (2006). Fate of outflowing suprathermal oxygen ions that originate in the polar ionosphere. *Journal of Geophysical Research*, *111*, A04219. <https://doi.org/10.1029/2005JA011403>
- Engwall, E., Eriksson, A. I., André, M., Dandouras, I., Paschmann, G., Quinn, J., & Torkar, K. (2006). Low-energy (order 10 eV) ion flow in the magnetotail lobes inferred from spacecraft wake observations. *Geophysical Research Letters*, *33*, L06110. <https://doi.org/10.1029/2005GL025179>
- Engwall, E., Eriksson, A. I., Cully, C. M., André, M., Puhl-Quinn, P. A., Vaith, H., & Torbert, R. (2009). Survey of cold ionospheric outflows in the magnetotail. *Annales Geophysicae*, *27*, 3185–3201. <https://doi.org/10.5194/angeo-27-3185-2009>
- Engwall, E., Eriksson, A. I., Cully, C. M., André, M., Torbert, R., & Vaith, H. (2009). Earth's ionospheric outflow dominated by hidden cold plasma. *Nature Geoscience*, *2*, 24–27. <https://doi.org/10.1038/ngeo387>
- Eriksson, A. I., André, M., Klecker, B., Laakso, H., Lindqvist, P.-A., Mozer, F., ... Vaith, H. (2006). Electric field measurements on Cluster: Comparing the double-probe and electron drift techniques. *Annales Geophysicae*, *24*, 275–289. <https://doi.org/10.5194/angeo-24-275-2006>
- Escoubet, C. P., Schmidt, R., & Goldstein, M. L. (1997). Cluster—Science and mission overview. *Space Science Reviews*, *79*, 11–32. <https://doi.org/10.1023/A:1004923124586>
- Förster, M., Paschmann, G., Haaland, S. E., Quinn, J. M., Torbert, R. B., Vaith, H., & Kletzing, C. A. (2007). High-latitude plasma convection from Cluster EDI: Variances and solar wind correlations. *Annales Geophysicae*, *25*, 1691–1707. <https://doi.org/10.5194/angeo-25-1691-2007>
- Friedrich, M., Egger, G., & Torkar, K. M. (2006). First results of the polar cap ionosphere based on EISCAT Svalbard and Heiss Island rocket data. *Advances in Space Research*, *37*, 1097–1101. <https://doi.org/10.1016/j.asr.2005.01.033>
- Glocer, A., Kitamura, N., Toth, G., & Gombosi, T. (2012). Modeling solar zenith angle effects on the polar wind. *Journal of Geophysical Research*, *117*, A04318. <https://doi.org/10.1029/2011JA017136>
- Gustafsson, G., Bostrom, R., Holback, B., Holmgren, G., Lundgren, A., Stasiewicz, K., ... Wygant, J. (1997). The electric field and wave experiment for the Cluster mission. *Space Science Reviews*, *79*, 137–156. <https://doi.org/10.1023/A:1004975108657>
- Haaland, S., André, M., Eriksson, A., Li, K., Nilsson, H., & Baddeley, L. (2016). *Low-energy ion outflow observed by Cluster* (pp. 33–47). Hoboken, NJ: John Wiley. <https://doi.org/10.1002/9781119066880.ch3>
- Haaland, S., Eriksson, A., André, M., Maes, L., Baddeley, L., Barakat, A., ... Welling, D. (2015). Estimation of cold plasma outflow during geomagnetic storms. *Journal of Geophysical Research: Space Physics*, *120*, 10,622–10,639. <https://doi.org/10.1002/2015JA021810>
- Haaland, S., Eriksson, A., Engwall, E., Lybakk, B., Nilsson, H., Pedersen, A., ... Østgaard, N. (2012). Estimating the capture and loss of cold plasma from ionospheric outflow. *Journal of Geophysical Research*, *117*, A07311. <https://doi.org/10.1029/2012JA017679>
- Huddleston, M. M., Chappell, C. R., Delcourt, D. C., Moore, T. E., Giles, B. L., & Chandler, M. O. (2005). An examination of the process and magnitude of ionospheric plasma supply to the magnetosphere. *Journal of Geophysical Research*, *110*, A12202. <https://doi.org/10.1029/2004JA010401>
- Johnson, M. T., & Wygant, J. R. (2003). The correlation of plasma density distributions over 5000 km with solar illumination of the ionosphere: Solar cycle and zenith angle observations. *Geophysical Research Letters*, *30*, 2260. <https://doi.org/10.1029/2003GL018175>
- Khazanov, G. V., Liemohn, M. W., & Moore, T. E. (1997). Photoelectron effects on the self-consistent potential in the collisionless polar wind. *Journal of Geophysical Research*, *102*, 7509–7522. <https://doi.org/10.1029/96JA03343>
- Kitamura, N., Ogawa, Y., Nishimura, Y., Terada, N., Ono, T., Shinbori, A., ... Smilauer, J. (2011). Solar zenith angle dependence of plasma density and temperature in the polar cap ionosphere and low-altitude magnetosphere during geomagnetically quiet periods at solar maximum. *Journal of Geophysical Research*, *116*, A08227. <https://doi.org/10.1029/2011JA016631>
- Lemaire, J., & Scherer, M. (1969). Le champ électrique de polarisation dans l'exosphère ionique polaire. *Comptes Rendus de l'Académie des Sciences, Série B*, *269*, 666–669. <https://doi.org/10.1029/JA074i014p03730>
- Lemaire, J., & Scherer, M. (1970). Model of the polar ion-exosphere. *Planetary and Space Science*, *18*, 103–120. [https://doi.org/10.1016/0032-0633\(70\)90070-X](https://doi.org/10.1016/0032-0633(70)90070-X)
- Lybakk, B., Pedersen, A., Haaland, S., Svenes, K., Fazakerley, A. N., Masson, A., ... Trotignon, J.-G. (2012). Solar cycle variations of the Cluster spacecraft potential and its use for electron density estimations. *Journal of Geophysical Research*, *117*, A01217. <https://doi.org/10.1029/2011JA016969>
- Maes, L., Maggiolo, R., & De Keyser, J. (2016). Seasonal variations and north-south asymmetries in polar wind outflow due to solar illumination. *Annales Geophysicae*, *34*, 961–974. <https://doi.org/10.5194/angeo-34-961-2016>
- Maes, L., Maggiolo, R., De Keyser, J., Dandouras, I., Fear, R. C., Fontaine, D., & Haaland, S. (2015). Solar illumination control of ionospheric outflow above polar cap arcs. *Geophysical Research Letters*, *42*, 1304–1311. <https://doi.org/10.1002/2014GL02972>
- Maggiolo, R., Echim, M., de Keyser, J., Fontaine, D., Jacquey, C., & Dandouras, I. (2011). Polar cap ion beams during periods of northward IMF: Cluster statistical results. *Annales Geophysicae*, *29*, 771–787.
- Maggiolo, R., Echim, M., Wedlund, C. S., Zhang, Y., Fontaine, D., Lointier, G., & Trotignon, J.-G. (2012). Polar cap arcs from the magnetosphere to the ionosphere: Kinetic modelling and observations by Cluster and TIMED. *Annales Geophysicae*, *30*, 283–302.

- Moore, T. E., Chappell, C. R., Chandler, M. O., Craven, P. D., Giles, B. L., Pollock, C. J., ... Mozer, F. S. (1997). High-altitude observations of the polar wind. *Science*, *277*, 349–351. <https://doi.org/10.1126/science.277.5324.349>
- Moore, T. E., & Khazanov, G. V. (2010). Mechanisms of ionospheric mass escape. *Journal of Geophysical Research*, *115*, A00J13. <https://doi.org/10.1029/2009JA014905>
- Nagai, T., Waite Jr., J. H., Green, J. L., Chappell, C. R., Olsen, R. C., & Comfort, R. H. (1984). First measurements of supersonic polar wind in the polar magnetosphere. *Geophysical Research Letters*, *11*, 669–672. <https://doi.org/10.1029/GL011i007p00669>
- Nilsson, H., Barghouthi, I. A., Slapak, R., Eriksson, A. I., & André, M. (2012). Hot and cold ion outflow: Spatial distribution of ion heating. *Journal of Geophysical Research*, *117*, A11201. <https://doi.org/10.1029/2012JA017974>
- Nishida, A. (1966). Formation of plasmopause, or magnetospheric plasma knee, by the combined action of magnetospheric convection and plasma escape from the tail. *Journal of Geophysical Research*, *71*, 5669–5679. <https://doi.org/10.1029/JZ071i023p05669>
- Nsumei, P. A., Reinisch, B. W., Song, P., Tu, J., & Huang, X. (2008). Polar cap electron density distribution from IMAGE radio plasma imager measurements: Empirical model with the effects of solar illumination and geomagnetic activity. *Journal of Geophysical Research*, *113*, A01217. <https://doi.org/10.1029/2007JA012566>
- Paschmann, G., Melzner, F., Frenzel, R., Vaith, H., Parigger, P., Pagel, U., ... Whipple, E. C. (1997). The electron drift instrument for Cluster. *Space Science Reviews*, *79*, 233–269. <https://doi.org/10.1023/A:1004917512774>
- Pedersen, A., Décréau, P., Escoubet, C.-P., Gustafsson, G., Laakso, H., Lindqvist, P.-A., ... Vaivads, A. (2001). Four-point high time resolution information on electron densities by the electric field experiments (EFW) on Cluster. *Annales Geophysicae*, *19*, 1483–1489.
- Pedersen, A., Lybekk, B., André, M., Eriksson, A., Masson, A., Mozer, F. S., ... Whipple, E. (2008). Electron density estimations derived from spacecraft potential measurements on Cluster in tenuous plasma regions. *Journal of Geophysical Research*, *113*, A07S33. <https://doi.org/10.1029/2007JA012636>
- Pollock, C. J., Chandler, M. O., Moore, T. E., Chappell, C. R., & Waite Jr, J. H. (1990). A survey of upwelling ion event characteristics. *Journal of Geophysical Research*, *95*, 18,969–18,980. <https://doi.org/10.1029/JA095iA11p18969>
- Strangeway, R. J., Ergun, R. E., Su, Y.-J., Carlson, C. W., & Elphic, R. C. (2005). Factors controlling ionospheric outflows as observed at intermediate altitudes. *Journal of Geophysical Research*, *110*, A03221. <https://doi.org/10.1029/2004JA010829>
- Su, Y.-J., Horwitz, J. L., Moore, T. E., Giles, B. L., Chandler, M. O., Craven, P. D., ... Pollock, C. J. (1998). Polar wind survey with the Thermal Ion Dynamics Experiment/Plasma Source Instrument suite aboard POLAR. *Journal of Geophysical Research*, *103*, 29,305–29,338. <https://doi.org/10.1029/98JA02662>
- Su, Y.-J., Horwitz, J. L., Wilson, G. R., Richards, P. G., Brown, D. G., & Ho, C. W. (1998). Self-consistent simulation of the photoelectron-driven polar wind from 120 km to 9 R_E altitude. *Journal of Geophysical Research*, *103*, 2279–2296. <https://doi.org/10.1029/97JA03085>
- Tsyganenko, N. A. (1989). A magnetospheric magnetic field model with a warped tail current sheet. *Planetary and Space Science*, *37*, 5–20. [https://doi.org/10.1016/0032-0633\(89\)90066-4](https://doi.org/10.1016/0032-0633(89)90066-4)
- Yau, A. W., & André, M. (1997). Sources of ion outflow in the high latitude ionosphere. *Space Science Reviews*, *80*, 1–25. <https://doi.org/10.1023/A:1004947203046>
- Yau, A. W., Peterson, W. K., & Shelley, E. G. (1988). *Quantitative parametrization of energetic ionospheric ion outflow*, *Geophysical Monograph Series* (Vol. 44, pp. 211–217). Washington, DC: American Geophysical Union. <https://doi.org/10.1029/GM044p0211>